

UNDERSTANDING EMITTANCE DILUTING EFFECTS IN HIGHLY OPTIMIZED ULTRAFAST ELECTRON DIFFRACTION BEAMLINES

C. M. Pierce, I. Bazarov, C. Gulliford, J. Maxson, Cornell University, Ithaca, NY, 14853, USA
S. Baturin, M. Gordon, Y. Kim, University of Chicago, Chicago, IL, 60637, USA

Abstract

The application of Multiobjective Genetic Algorithm optimization (MOGA) to photoemission based ultrafast electron diffraction (UED) beamlines featuring extremely low cathode mean transverse energies has lead to designs with emittances as low as 1 nm for sub-picosecond bunches with 10^5 electrons [1]. Analysis of these results shows significant emittance growth during transport: with emittance dilution as high as a factor of 200-4000% for various designs and optics settings. In this study we quantify and model the individual sources of emittance growth (slice mismatches and space charge), and explore the use of the core emittance as a strong invariant.

INTRODUCTION

The study of biological samples using Ultrafast Electron Diffraction (UED), such as proteins, remains challenging for single-shot experiments, as they require high transverse coherence, extremely short pulses, and sufficient bunch charges [2]. Recent advances in low MTE photocathodes have the potential to deliver beams with these characteristics. In order to make efficient use of these cathodes, care must be taken during the space charge dominated transport to preserve the initial low emittances produced by these cathodes.

In previous work [1], MOGA was applied to 3D space charge simulations (using General Particle Tracer (GPT) [3, 4]) of the cryogun beamline under commissioning at Cornell [1, 5-7] in order to determine the limitations of the emittance performance from an extremely low MTE cathode. This setup features a 225 kV DC gun housing a cryogenically cooled cathode with an (projected) MTE of 5 meV and a 3 GHz normal conducting buncher cavity field map between two solenoid magnets. The intended sample location is located at roughly 1 m from that cathode (the exact position varies slightly among the different optimized solutions). A typical field profile is shown in Fig. 1.

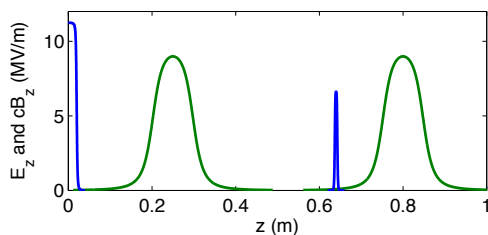


Figure 1: Generic on-axis electric field E_z (blue) and solenoid field B_z (green) profiles for the cryogun set-up. The intended sample location is at roughly 1 m.

In all simulations, the optimizer varied the beamline parameters, element positions, and arbitrarily shaped both the transverse and longitudinal laser distributions. The resulting

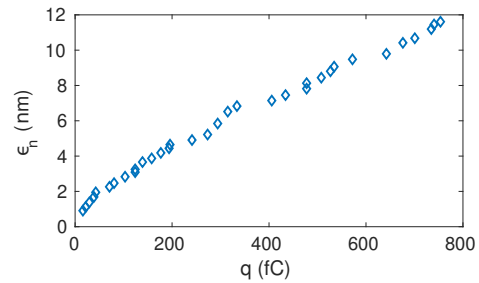


Figure 2: The optimal emittances as a function of bunch charge at the sample location (roughly 1 m).

optimal emittance as a function of bunch charge is shown in Fig. 2. In this work, we focus on two example cases from this front corresponding to charges of 10^5 and 10^6 electrons. For these examples the corresponding intended sample locations are 1.0 m and 0.95 m from the cathode. The initial/final emittance at the sample location was 0.33/0.81 (0.89/5) nm for the 10^5 (10^6) bunch charges, corresponding to an emittance growth of 145%, and 460%, respectively.

PROJECTED EFFECTS

In analyzing the emittance growth in the two example beamlines, we first consider any remaining possible sources of projected emittance growth. This contribution is divided into two components: slice misalignment, and slice size mismatch. Here, misalignment refers to the spread of the slopes in the transverse phase spaces (p_x vs. x and p_y vs. y), while mismatch refers to differences in the rms sizes in each phase space coordinate. Fig. 3 shows the combined effect of these two contributions by plotting the ratio of the full emittance to the average slice emittance. 50 longitudinal slices were used in this calculation. In the 10^5 electron case, the total projected emittance grows substantially compared to the average slice emittance, however this is nearly completely compensated. The situation is different for the 10^6 electron example, where the ratio grows quickly at the beginning and then is partially compensated at the end of the beamline. We anticipate that this is due to space charge, and is investigated in the following section.

In order to determine the lowest possible emittance from ideal linear emittance compensation, the extent of slice mismatch and slice misalignment at the end of the beamline have been computed. To do this, the final beam was sliced into 50 longitudinal slices of equal length and the x - p_x and

Content from this work may be used under the terms of the CC BY 3.0 licence (© 2018). Any distribution of this work must maintain attribution to the author(s), title of the work, publisher, and DOI.

Table 1: Summary of the Causes of Emittance Growth in Representative UED Beamlines.

Charge	Slice Contribution	Dominant Emittance Component	Core Emittance Growth
10^5 Electrons	15.4%	Space Charge	7.8%
10^6 Electrons	44.4%	Space Charge	21%

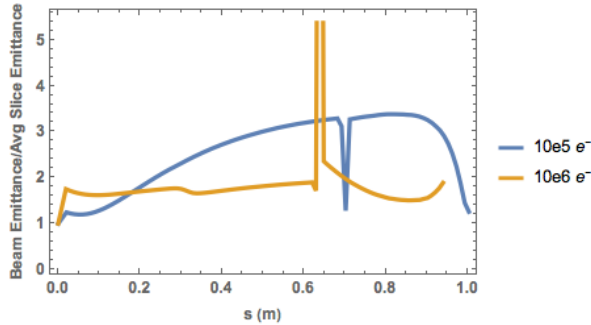


Figure 3: Ratio of the beam emittance to the average slice emittance (50 slices) for the two example charges.

y - p_y correlations calculated. The values of p_x and p_y of each particle were then adjusted to remove the individual slice slope. Next, the spreads in position and momentum were calculated for the slices, as well as the full beam. The spread in position space of each slice was then replaced by the spread in position space of the beam. The spread in momentum space was then proportionally changed for each slice to preserve individual slice emittance. Lastly, each particle's p_x and p_y were changed to make each slice's slope equal to the beam slope.

Before applying this method, the transverse emittance of the beam in the 10^5 (10^6) electron case was 0.858 nm (4.90 nm) at the end of the beamline. After the removal of slice effects, this was reduced to 0.727 nm (2.73 nm). This corresponds to a 15.4% (44.4%) reduction of the final beam emittance if these effects could be removed. This is consistent with figure 3 which at the end of the beamline shows the slice emittance is 17% (47%) smaller than the beam emittance.

EMITTANCE CONTRIBUTIONS

The reduction in the emittance is fundamentally limited by the individual slice emittances, which grow in the presence of non-linear forces, like those arising from space charge. Thus it is important to analyze the effects of space charge to the emittance. To do so, we have developed a method to associate a contribution to the final emittance from each internal or applied force. We first exploit the fact the space charge and external fields are cylindrically symmetric, and thus we may express the uncorrelated 2D transverse emittance as

$$\epsilon_n = \frac{1}{m_0 c} |\Sigma_4|^{1/4}, \quad (1)$$

where $\Sigma_4 = \langle \vec{u}_4 \vec{u}_4^T \rangle$ is the 4D transverse correlation matrix for the phase space coordinates $\vec{u}_4 = [x, p_x, y, p_y]^T$. The average, denoted by $\langle \dots \rangle$, is taken over the 4D transverse

particle distribution $\rho_4 = \rho_4(x, p_x, y, p_y)$, and assumes no coupling to the longitudinal coordinates. This expression will prove useful in analyzing the growth of individual slice emittances along the beam. The time derivative of the emittance in Eq. 1 may be expressed, using matrices, as

$$\dot{\epsilon}_n = \frac{1}{4m_0^4 c^4 \epsilon_n^3} \text{tr}(\text{adj}(\Sigma_4) \dot{\Sigma}_4), \quad (2)$$

where the time derivative of the correlation matrix is given explicitly by

$$\dot{\Sigma}_4 = 2 \cdot \text{sym} \langle \vec{u}_4 \cdot [v_x, F_x, v_y, F_y] \rangle. \quad (3)$$

The matrix $\dot{\Sigma}_4$ is linear in the row vector in Eq. 3 and may be separated into three components that sum to $\dot{\Sigma}_4$.

$$\dot{\Sigma}_{\text{Ext}} = 2 \cdot \text{sym} \langle \vec{u}_4 \cdot [0, F_{x,\text{Ext}}, 0, F_{y,\text{Ext}}] \rangle, \quad (4)$$

$$\dot{\Sigma}_{\text{SC}} = 2 \cdot \text{sym} \langle \vec{u}_4 \cdot [0, F_{x,\text{SC}}, 0, F_{y,\text{SC}}] \rangle, \quad (5)$$

$$\dot{\Sigma}_{\text{NF}} = 2 \cdot \text{sym} \langle \vec{u}_4 \cdot [v_x, 0, v_y, 0] \rangle. \quad (6)$$

Here F_{Ext} and F_{SC} denote the external beamline element and space charge fields, respectively. The last term $\dot{\Sigma}_{\text{NF}}$ is identified as the non-force contribution to $\dot{\Sigma}_4$, and arises from any break down of the paraxial approximation (for example, from very large energy spread).

A custom GPT element was created to numerically evaluate the emittance growth components within each GPT simulation. Figure 4 shows the value of these components as a function of time for typical examples of the UED beamlines being studied. The space charge component of emittance dominates the emittance at the target location. This result implies that non-linear space charge forces are an important limiting factor in the UED beamline being studied.

CORE EMITTANCE INVARIANCE

It follows from Liouville's theorem that the uncorrelated transverse core emittance, given by:

$$\epsilon_{n,\text{core}} \propto \rho_4^{-1/2}(x, p_x, y, p_y) \Big|_{x,y,p_x,p_y=0}, \quad (7)$$

is a strong invariant, provided there is no transverse-to-longitudinal coupling. The algorithm to compute the core emittance used in this work is a two step process. First, the particle phase space coordinates \vec{u}_4 are transformed to uncorrelated variables by diagonalizing Σ_4 . The distribution can then be written as $\rho_4 \rightarrow \hat{\rho}_4 = \hat{\rho}_4(\hat{r})$ where \hat{r} is the "radial" coordinate of the uncorrelated phase space variables. The average of \hat{r} is computed and the process repeated using a

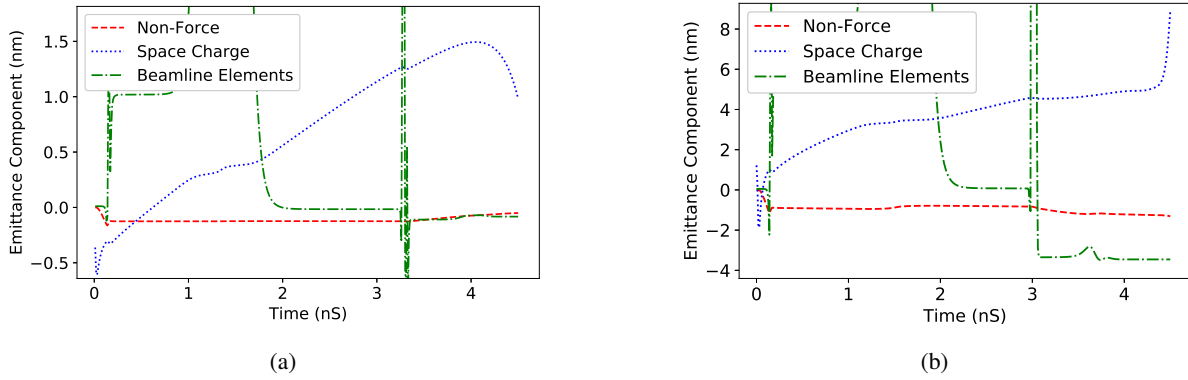


Figure 4: Emittance growth components along representative UED beamlines. a) Beamline optimized for 10^5 electrons. Sample located at 4.8 ns. b) Beamline optimized for 10^6 electrons. Sample located at 4.6 ns.

subset of the phase space region defined by $\hat{r} \leq f \cdot \hat{r}_{avg}$, where $f < 1$ ($f = 0.3$ in calculations shown here), resulting in a final uncorrelated distribution $\tilde{\rho}_4$ near the phase space origin. $\tilde{\rho}_4(\vec{r})$ is then extrapolated to $\vec{r} = 0$ giving $\tilde{\rho}_4(\vec{r} = 0) = \rho_4(\vec{u}_4 = 0)$.

This method relies on sampling ρ_4 near the phase space origin, and is sensitive to the particle density there. For the examples used here, convergence of this quantity required the macroparticle count to be $\geq 20k$. Fig. 5 shows the core emittance evolution for both the 10^5 and 10^6 electron examples Fig. 5 These plots were computed using 10^5 and 10^6

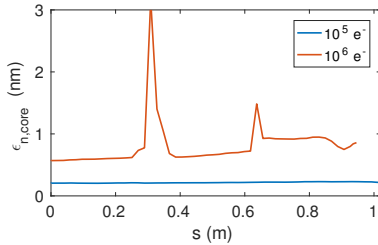


Figure 5: Core emittance along the beamline for both example cases.

macroparticles for the 10^5 and 10^6 electrons per bunch examples, respectively. The core emittance growth evaluated at the optimization point was 7.8% and 21% respectively, implying this quantity is a strongly conserved quantity. Further analysis is underway to determine the cause of the core emittance spikes seen in the 10^6 case. Note that these occur at the solenoid and buncher locations.

CONCLUSION

Table 1 contains the results of each analysis for the two example beamlines. These results suggest that space charge is the limiting factor in the UED beamlines under study. Analysis using the emittance growth components shows space charge is responsible for a large growth in emittance early on in the beamline that remains largely uncorrected at the target. While the removal of slice effects has been shown to improve the final emittance by as much as 45%, this

likely not a limit on the emittance performance of the example beamlines. Additionally, these results show that the core emittance provides a strong transport invariant, and warrants further investigation. Those seeking to get the most performance from UED setups employing modern low MTE photocathodes must find methods to avoid or compensate for emittance dilution, particularly growth due to space charge effects.

ACKNOWLEDGMENT

This work was supported by the Center for Bright Beams, NSF PHY-1549132 and Department of Energy grant DE-SC0014338.

REFERENCES

- [1] Colwyn Gulliford, Adam Bartnik, and Ivan Bazarov. Multi-objective optimizations of a novel cryocooled dc gun based ultrafast electron diffraction beam line. *Physical Review Accelerators and Beams*, 19(9):093402, 2016.
- [2] R. K. Li, K. G. Roberts, C. M. Scoby, H. To, and P. Musumeci. Femtosecond electron diffraction: Heraldng the era of atomically resolved dynamics. *Rep. Prog. Phys.*, 74:096101, 2011.
- [3] Pulsar website for gpt. <http://www.pulsar.nl/gpt/>, 2011.
- [4] S.B. van der Geer, M.J. de Loos O.J. Luiten, G. Pöplau, and U. van Rienen. Institute of physics conference series. Number 175, page 101, 2005.
- [5] T. van Oudheusden, E. F. de Jong, S. B. van der Geer, W. P. E. M. Op 't Root, O. J. Luiten, and B. J. Siwick. Electron source concept for single-shot sub-100 fs electron diffraction in the 100 keV range. *Journal of Applied Physics*, 102(9):-, 2007.
- [6] Robert P. Chatelain, Vance R. Morrison, Chris Godbout, and Bradley J. Siwick. Ultrafast electron diffraction with radio-frequency compressed electron pulses. *Applied Physics Letters*, 101(8):-, 2012.
- [7] T. van Oudheusden, P. L. E. M. Pasmans, S. B. van der Geer, M. J. de Loos, M. J. van der Wiel, and O. J. Luiten. Compression of subrelativistic space-charge-dominated electron bunches for single-shot femtosecond electron diffraction. *Phys. Rev. Lett.*, 105:264801, Dec 2010.